

Eigenvalue distributions of large Euclidean random matrices for waves in random media

S E Skipetrov and A Goetschy

Laboratoire de Physique et Modélisation des Milieux Condensés, Université Joseph Fourier and CNRS UMR 5493, B.P. 166, 25 rue des Martyrs, Maison des Magistères, 38042 Grenoble Cedex 09, France

E-mail: Sergey.Skipetrov@grenoble.cnrs.fr

Abstract. We study probability distributions of eigenvalues of Hermitian and non-Hermitian Euclidean random matrices that are typically encountered in the problems of wave propagation in random media.

PACS numbers: 42.25.Dd, 02.50.Cw, 05.40.-a

1. Introduction

Random matrix theory is a powerful tool of statistical physics [1] with important applications in the field of quantum and wave transport in random media [2, 3, 4]. A special class of random matrices are Euclidean random matrices with elements F_{ij} defined with the help of some function $f(\mathbf{r}_i, \mathbf{r}_j)$: $F_{ij} = f(\mathbf{r}_i, \mathbf{r}_j)$. Here \mathbf{r}_i ($i = 1, \dots, N$) are randomly chosen points in the Euclidean space [5, 6]. The purpose of this paper is to study eigenvalue distributions of certain large Euclidean random matrices that appear in problems of wave propagation in random media. Because in the simplest case of scalar waves the propagation is described by a scalar wave equation, the function f that will be of interest to us is the Green's function $G(\mathbf{r}_i, \mathbf{r}_j)$ of the Helmholtz equation

$$(\nabla^2 + k_0^2 + i\eta) G(\mathbf{r}_i, \mathbf{r}_j) = -\frac{4\pi}{k_0} \delta(\mathbf{r}_i - \mathbf{r}_j), \quad (1)$$

where η is a positive infinitesimal. It is easy to see that $G(\mathbf{r}_i, \mathbf{r}_j) = \exp(ik_0|\mathbf{r}_i - \mathbf{r}_j|)/k_0|\mathbf{r}_i - \mathbf{r}_j|$ ‡.

Statistical properties of the ensemble of matrices \hat{G} with elements $G_{ij} = (1 - \delta_{ij})G(\mathbf{r}_i, \mathbf{r}_j)$ for $N \gg 1$ are of primary importance in the context of Anderson localization of electromagnetic [7, 8, 9] and matter [10] waves. The same matrices appear in the studies of Dicke superradiance in dense atomic systems [11, 12, 13, 14, 15]. The interplay between Anderson localization and Dicke superradiance can also be described by this ensemble of matrices [16] and properties of their eigenvalues are important for understanding of random lasers [17, 18]. Meanwhile, the matrix \hat{G} is non-Hermitian,

‡ We restrict ourselves to three-dimensional space in this paper.

its eigenvalues are complex and their probability distribution is difficult to access. This is why in several works dealing with superradiance [12, 14, 15, 16] the imaginary part of \hat{G} , a matrix with elements $\sin(k_0|\mathbf{r}_i - \mathbf{r}_j|)/k_0|\mathbf{r}_i - \mathbf{r}_j|$, was considered. This real symmetric matrix is much easier to study and in many situations it still contains some of the important aspects of the full problem. Similarly, the real part of \hat{G} , a matrix with elements $\cos(k_0|\mathbf{r}_i - \mathbf{r}_j|)/k_0|\mathbf{r}_i - \mathbf{r}_j|$, is relevant for understanding the collective Lamb shifts in dense atomic systems [13, 15].

Despite the importance of the three matrices \hat{G} , $\text{Im}\hat{G}$ and $\text{Re}\hat{G}$ introduced above little is known about statistical properties of their eigenvalues. In the general case, the eigenvalue distribution of \hat{G} was studied only numerically [7, 8, 9]. Analytic results are available for \hat{G} , $\text{Im}\hat{G}$ and $\text{Re}\hat{G}$ in the limit of high density of points \mathbf{r}_i inside a sphere: $\rho = N/V \rightarrow \infty$ [12, 13, 14, 15], when the summation in the eigenvalue equation $\sum_j G_{ij}\psi_j = \lambda\psi_i$ can be replaced by an integration. The purpose of this paper is to partially fill this gap by considering eigenvalue distributions of the three matrices above in the case of low and intermediate densities ρ , when the distances between points \mathbf{r}_i are larger than or comparable to the wavelength $\lambda_0 = 2\pi/k_0$. This situation is of particular importance in the context of wave propagation in random media. Indeed, for an ensemble of point scatterers located at points \mathbf{r}_i , the eigenvalues of \hat{G} determine the frequencies and the life times of quasi-modes of the corresponding Helmholtz equation. On the one hand, a possible experimental realization of such a system is a cloud of cold atoms in which propagation of quasi-resonant light (wavelength λ_0) is studied §. Nowadays such clouds are routinely created at densities $\rho\lambda_0^3 \ll 1$, allowing observation of interesting phenomena due to the multiple scattering of light [19, 20]. This justifies the importance of properly understanding the low-density regime. On the other hand, the most interesting phenomena for waves in an ensemble of point-like scattering centers are known to take place at densities $\rho\lambda_0^3 \gtrsim 1$, when interference effects become important, eventually leading to Anderson localization of waves (see, e.g., [21] and references therein). Our results may be useful for understanding Anderson localization and its interplay with other collective phenomena (such as Dicke superradiance) [16].

2. General framework

Consider a singly-connected three-dimensional region of space V . Let $\{\psi_m(\mathbf{r})\}$ be an orthonormal basis in V , such that

$$\int_V d^3\mathbf{r} \psi_m(\mathbf{r})\psi_n^*(\mathbf{r}) = \delta_{mn}. \quad (2)$$

We will now show that an arbitrary $N \times N$ Euclidean random matrix \hat{F} with elements

$$F_{ij} = f(\mathbf{r}_i, \mathbf{r}_j), \quad i, j = 1, \dots, N, \quad (3)$$

§ Light is a vector wave but here we restrict ourselves to a scalar approximation.

where f is an arbitrary, sufficiently well-behaved function of $\mathbf{r}_i, \mathbf{r}_j \in V$, can be represented as

$$\hat{F} = \hat{H}\hat{T}\hat{H}^\dagger. \quad (4)$$

Here \hat{H} is a $N \times M$ matrix with elements

$$H_{im} = \sqrt{\frac{V}{N}}\psi_m(\mathbf{r}_i) \quad (5)$$

(we use V to denote the volume of the considered three-dimensional region as well), \hat{T} is a $M \times M$ matrix to be defined below, and the dagger “ \dagger ” denotes Hermitian conjugation.

To establish Eq. (4), we write the ij 'th element of the matrix \hat{F} explicitly as

$$F_{ij} = \frac{V}{N} \sum_{m,n} T_{mn} \psi_m(\mathbf{r}_i) \psi_n^*(\mathbf{r}_j), \quad (6)$$

where we used Eq. (5) and the definition of matrix multiplication. Multiplying this equation by $\psi_{m'}^*(\mathbf{r}_i) \psi_{n'}(\mathbf{r}_j)$, integrating over \mathbf{r}_i and \mathbf{r}_j , and using the orthogonality of the basis functions $\psi_m(\mathbf{r})$, we readily obtain

$$T_{mn} = \frac{N}{V} \int_V d^3\mathbf{r}_i \int_V d^3\mathbf{r}_j f(\mathbf{r}_i, \mathbf{r}_j) \psi_m^*(\mathbf{r}_i) \psi_n(\mathbf{r}_j). \quad (7)$$

We see that \hat{T} is, in principle, a matrix of infinite dimension M . It is easy to check that with the elements T_{mn} of \hat{T} defined by Eq. (7), Eq. (4) is indeed obeyed.

When the points $\{\mathbf{r}_i\}$ are chosen inside V randomly, \hat{F} and \hat{H} become random matrices, whereas \hat{T} is always a non-random matrix independent of $\{\mathbf{r}_i\}$ and determined uniquely by the function f , the region V , and the choice of the orthonormal basis $\{\psi_m(\mathbf{r})\}$. Moreover, the elements H_{im} of \hat{H} are independent random variables with variances equal to $1/N$. The representation (4) is therefore very useful because it can be dealt with using the powerful mathematical arsenal of the so-called free random variable theory [22, 23, 26]. Without going into details, we remind the reader that for random matrices, the notion of asymptotic freeness [22] is equivalent to the notion of statistical independence that we are familiar with for random variables. Three fundamental objects of the free random variable theory will be useful for us in this paper: the usual Green's function $\mathcal{G}(z)$, the Blue function $B(z)$ equal to the functional inverse of $\mathcal{G}(z)$:

$$B[\mathcal{G}(z)] = z, \quad (8)$$

and the S -transform of the probability distribution of eigenvalues defined through an auxiliary function $\chi(z)$:

$$S(z) = \frac{1+z}{z} \chi(z), \quad (9a)$$

$$\frac{1}{\chi(z)} \mathcal{G} \left[\frac{1}{\chi(z)} \right] - 1 = z. \quad (9b)$$

If the two Hermitian random matrices \hat{A} and \hat{B} are asymptotically free, the Blue function $B_{\hat{C}}(z)$ of their sum $\hat{C} = \hat{A} + \hat{B}$ is equal to the sum of individual Blue functions $B_{\hat{A}}(z)$

and $B_{\hat{B}}(z)$, minus $1/z$. The S -transform of the product $\hat{C} = \hat{A}\hat{B}$ can be found by multiplying the individual S -transforms of \hat{A} and \hat{B} . Once the Blue function or the S -transform corresponding to the random matrix \hat{C} are found, its Green's function $\mathcal{G}(z)$ can be calculated either from (8) or from (9a) and (9b). The probability density of the eigenvalues λ of \hat{C} is then determined in the usual way:

$$p(\lambda) = -\frac{1}{\pi} \lim_{\epsilon \rightarrow 0^+} \text{Im} \mathcal{G}(\lambda + i\epsilon). \quad (10)$$

The functions $\mathcal{G}(z)$, $B(z)$ and $S(z)$ all contain the same full information about the statistical distribution of eigenvalues λ as $p(\lambda)$. The Green's function can be represented as a series with coefficients in front of consecutive powers of $1/z$ equal to statistical moments of λ : $\mathcal{G}(z) = \sum_{n=0}^{\infty} \langle \lambda^n \rangle / z^{n+1}$. We have, therefore,

$$\langle \lambda^n \rangle = \frac{1}{(n+1)!} \left. \frac{d^{n+1} \mathcal{G}(z)}{d(1/z)^{n+1}} \right|_{z \rightarrow \infty}, \quad (11)$$

where z is assumed real. Using this equation and (8) we readily derive an expression for $\langle \lambda^n \rangle$ in terms of $B(z)$:

$$\langle \lambda^n \rangle = \frac{1}{(n+1)!} \left[-\frac{B^2(z)}{B'(z)} \frac{d}{dz} \right]^n \left[-\frac{B^2(z)}{B'(z)} \right] \Big|_{z \rightarrow 0}, \quad (12)$$

where $B'(z) = dB(z)/dz$. If we introduce the R -transform $\mathcal{R}(z) = B(z) - 1/z$ [23], the average eigenvalue and the second central moment simplify: $\langle \lambda \rangle = \mathcal{R}(0)$ and $\langle (\lambda - \langle \lambda \rangle)^2 \rangle = \mathcal{R}'(z)|_{z \rightarrow 0}$.

For matrices \hat{F} of the form (4), the free random variable theory provides a number of mathematical theorems that we will exploit in this paper. In particular, one shows [23] that

$$S_{\hat{F}}(z) = \frac{1}{z + M/N} S_{\hat{T}} \left(\frac{N}{M} z \right), \quad (13)$$

if \hat{T} is a Hermitian nonnegative random matrix independent of \hat{H} and the limits $N, M \rightarrow \infty$ are taken at a constant M/N . Using (13), we derive a relation between the Blue function of \hat{F} and the Green's function of \hat{T} :

$$B_{\hat{F}}(z) = \frac{1}{z} \left\{ 1 + \frac{M}{N} \left[\frac{1}{z} \mathcal{G}_{\hat{T}} \left(\frac{1}{z} \right) - 1 \right] \right\}. \quad (14)$$

A particular case that we will consider in the remainder of this paper is when the region V is a square box of side L [see figure 1(a)]. A convenient set of basis functions is then given by ‘‘plane waves’’

$$\psi_m(\mathbf{r}) = \frac{1}{\sqrt{V}} e^{i\mathbf{q}_m \cdot \mathbf{r}}, \quad (15)$$

where $\mathbf{q}_m = \{q_{m_x}, q_{m_y}, q_{m_z}\}$, $q_{m_x} = m_x \Delta q$ with $m_x \in \mathbb{Z}$ (and similarly for q_{m_y} and q_{m_z}), and $\Delta q = 2\pi/L$. Equation (7) is then simply a double Fourier transform of the function $f(\mathbf{r}_i, \mathbf{r}_j)$ in the box and the representation (4) stems from the Fourier series expansion of $f(\mathbf{r}_i, \mathbf{r}_j)$.

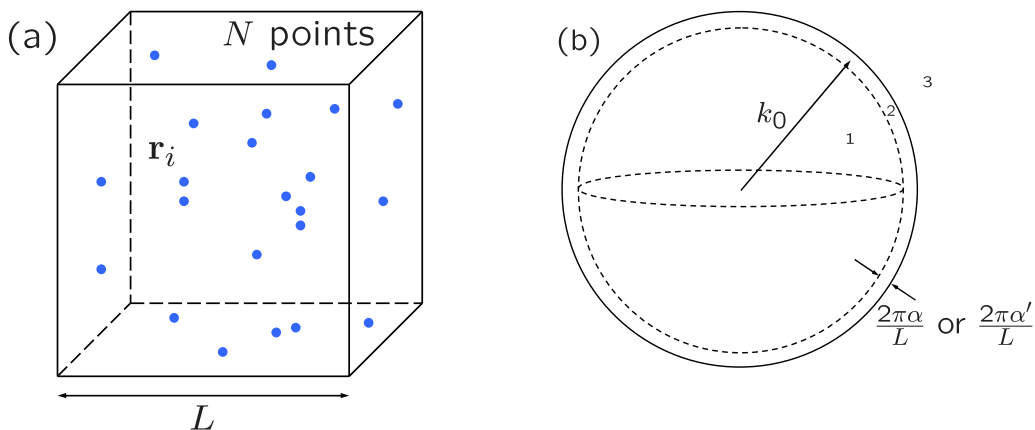


Figure 1. (a) We consider N points randomly distributed in a three-dimensional cube of side L . (b) Regions in the Fourier space. For the sinc random matrix, only the region 2 contribute to the matrix \hat{T} . In contrast, for the cosc random matrix, \hat{T} has contributions from the regions 1 and 3 but not from the region 2.

3. Eigenvalue distribution of the sinc matrix

We start by considering the real symmetric $N \times N$ Euclidean matrix $\hat{F} = \hat{S}$ with elements defined through the cardinal sine (sinc) function:

$$S_{ij} = f(\mathbf{r}_i - \mathbf{r}_j) = \frac{\sin(k_0|\mathbf{r}_i - \mathbf{r}_j|)}{k_0|\mathbf{r}_i - \mathbf{r}_j|}. \quad (16)$$

Here k_0 is a constant and the vectors \mathbf{r}_i define positions of N randomly chosen points inside a three-dimensional cube of side L .

The first important property of the matrix \hat{S} is the positiveness of its eigenvalues: $\lambda > 0$. Indeed, the Fourier transform of the function $f(\Delta\mathbf{r})$ in (16) is positive and hence $f(\Delta\mathbf{r})$ is a function of positive type. An Euclidean matrix defined through a function of positive type is positive definite and hence has only positive eigenvalues. The matrix \hat{T} corresponding to \hat{S} can be found from (7):

$$T_{mn} = \frac{N}{V^2} \int_V d^3\mathbf{r}_1 \int_V d^3\mathbf{r}_2 \frac{\sin(k_0|\mathbf{r}_1 - \mathbf{r}_2|)}{k_0|\mathbf{r}_1 - \mathbf{r}_2|} e^{-i\mathbf{q}_m\mathbf{r}_1 + i\mathbf{q}_n\mathbf{r}_2}. \quad (17)$$

Unfortunately, it is impossible to calculate this double integral exactly. However, introducing new variables of integration $\mathbf{R} = \frac{1}{2}(\mathbf{r}_1 + \mathbf{r}_2)$ and $\Delta\mathbf{r} = \mathbf{r}_2 - \mathbf{r}_1$ and extending the integration over $\Delta\mathbf{r}$ over the whole space, we obtain

$$\begin{aligned} T_{mn} &\simeq \frac{N}{V^2} \int_V d^3\mathbf{R} e^{-i(\mathbf{q}_m - \mathbf{q}_n)\mathbf{R}} \int d^3\Delta\mathbf{r} \frac{\sin(k_0\Delta r)}{k_0\Delta r} e^{i(\mathbf{q}_m + \mathbf{q}_n)\Delta\mathbf{r}/2} \\ &= \frac{2\pi^2 N}{k_0^2 V} \delta_{mn} \delta(q_m - k_0). \end{aligned} \quad (18)$$

On the one hand, because \mathbf{q}_m only takes discrete values, its absolute value q_m may coincide with k_0 only for certain well-defined box sizes L . For all other L 's T_{mn} given by (18) is equal to zero. On the other hand, the appearance of the delta-function $\delta(q_m - k_0)$

in (18) is due to the (unjustified) extension of the integration over $\Delta \mathbf{r}$ to the whole space. In reality, Δr cannot exceed $\sqrt{3}L$ and hence, in a more refined treatment, the delta-function in (18) would become a peaked function of finite width $\sim 1/L$. To mimic this feature, we replace $\delta(q_m - k_0)$ by a boxcar function $(L/2\pi\alpha)\Pi[(q_m - k_0)L/2\alpha\pi]$, where $\Pi(x) = 1$ for $|x| < \frac{1}{2}$ and $\Pi(x) = 0$ otherwise. Here $\alpha \sim 1$ is a numerical constant to be fixed later. We then obtain

$$T_{mn} \simeq \frac{2\pi^2 N}{k_0^2 V} \frac{L}{2\alpha\pi} \Pi \left[(q_m - k_0) \frac{L}{2\pi\alpha} \right] \delta_{mn} \quad (19)$$

which is different from zero only for \mathbf{q}_m 's inside a spherical shell of radius k_0 and thickness $2\pi\alpha/L$ [i.e. in the region 2 on figure 1(b)]. In addition, for all \mathbf{q}_m 's inside the shell the value of T_{mn} is the same and equal to N/M with $M = \alpha(k_0 L)^2/\pi \gg 1$ the number of \mathbf{q}_m 's inside the shell. Equation (4) then yields

$$\hat{S} = \frac{N}{M} \hat{H} \hat{H}^\dagger \quad (20)$$

which is equivalent to (4) with a $M \times M$ matrix $\hat{T} = (N/M)\mathbb{I}$. We then readily find $\mathcal{G}_{\hat{T}}(z) = (1/M) \text{Tr}(z - N/M)^{-1} = (z - N/M)^{-1}$ and from (14): $B_{\hat{S}}(z) = (1 - \beta z)^{-1} + 1/z$ with $\beta = N/M$. This is the Blue function of the famous Marchenko-Pastur law [24, 23]:

$$p(\lambda) = \left(1 - \frac{1}{\beta}\right)^+ \delta(\lambda) + \frac{\sqrt{(\lambda - \lambda_{\min})^+ (\lambda_{\max} - \lambda)^+}}{2\pi\beta\lambda} \quad (21)$$

where $\lambda_{\min, \max} = (1 \mp \sqrt{\beta})^2$ and $x^+ = \max(x, 0)$. The distribution of eigenvalues of the matrix (16) is therefore parameterized by a single parameter β equal to the variance of this distribution, as it is easy to check from (21): $\text{var}(\lambda) = \beta$.

Note that despite the fact that our derivation of (21) was based on several approximations, the average value of λ , $\langle \lambda \rangle = 1$, following from this equation is exact. The second moment of λ can also be found directly from (16). For $k_0 L \gg 1$ and in the limit $N \rightarrow \infty$ we find:

$$\langle \lambda^2 \rangle = \frac{1}{N} \langle \text{Tr} \hat{S}^2 \rangle = 1 + \frac{aN}{(k_0 L)^2}, \quad (22)$$

where the numerical constant a is given by

$$a = \frac{1}{2} \int_{\text{unit cube}} d^3 \mathbf{u}_1 \int_{\text{unit cube}} d^3 \mathbf{u}_2 \frac{1}{|\mathbf{u}_1 - \mathbf{u}_2|^2} \simeq 2.8, \quad (23)$$

with the integrations running over the volume of a cube of unit side. By requiring that the second moment $1 + \beta$ of the distribution (21) coincides with (22) we can now fix the value of α that remained arbitrary until now. We obtain $\alpha = \pi/a \simeq 1.12$ and

$$\beta = \frac{2.8N}{(k_0 L)^2}. \quad (24)$$

In figure 2 we present a comparison of Eq. (21) with the results of direct numerical simulations. The latter amount to generate N random points \mathbf{r}_i inside a three-dimensional cube, to use these points to define a random $N \times N$ matrix \hat{S} according to (16), and to diagonalize \hat{S} using the standard software package LAPACK [31]. The

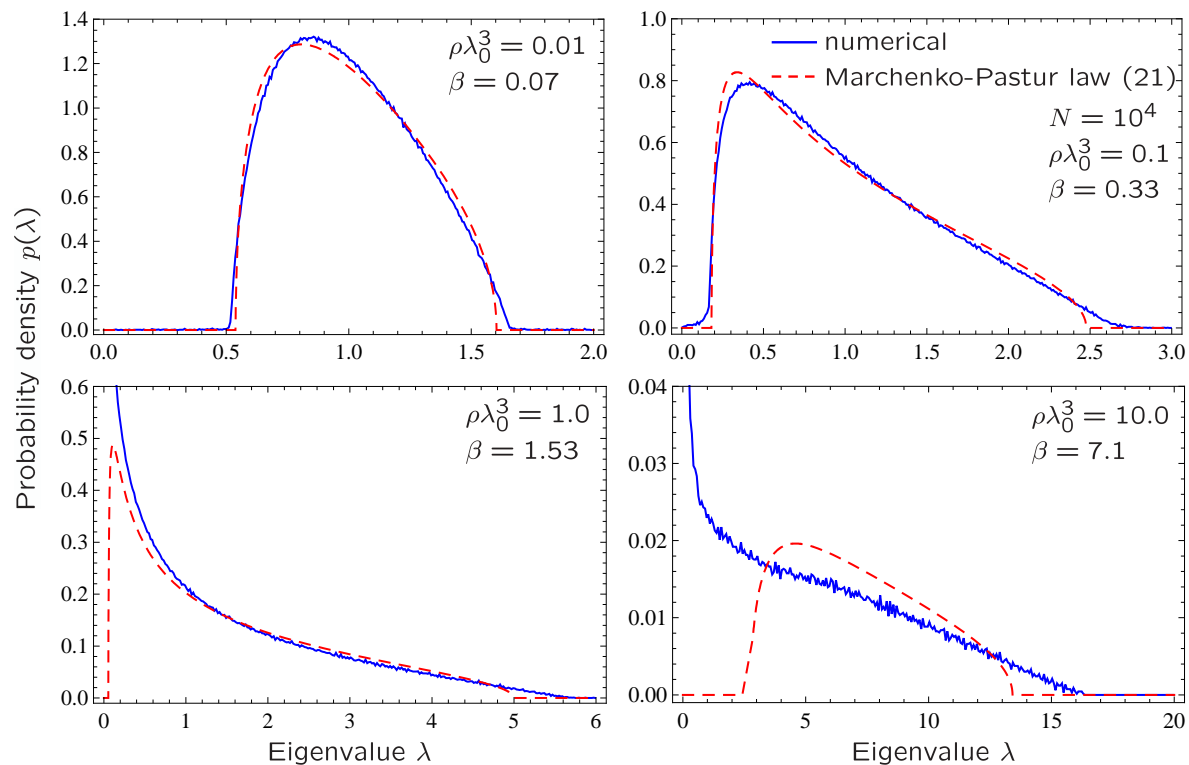


Figure 2. Probability density of eigenvalues of a square $N \times N$ Euclidean matrix \hat{S} with elements $S_{ij} = \sin(k_0|\mathbf{r}_i - \mathbf{r}_j|)/k_0|\mathbf{r}_i - \mathbf{r}_j|$, where the N points \mathbf{r}_i are randomly chosen inside a 3D cube of side L . Numerical results (blue solid lines) obtained for $N = 10^4$ after averaging over 10 realizations are compared to the Marchenko-Pastur law (21) (red dashed lines) with $\beta = 2.8N/(k_0L)^2$ for several densities ρ of points ($\lambda_0 = 2\pi/k_0$).

procedure is repeated several times and a histogram of all eigenvalues λ is created. This histogram approximates the eigenvalue distribution $p(\lambda)$. As we see from figure 2, the agreement between numerical results and the Marchenko-Pastur law (21) is good for $\beta < 1$ but (21) fails to describe $p(\lambda)$ when β becomes larger than unity. The reason for this is easy to understand if we go back to (17), (18) and (19). Indeed, when we approximate the result of integration in (17) by (19), we reduce the infinite-size matrix \hat{T} to a matrix of finite size $M \times M$. By definition, the rank of the latter matrix is inferior or equal to M . The rank of $\hat{S} = \hat{H}\hat{T}\hat{H}^\dagger$ cannot be larger than the rank of \hat{T} and hence is also bounded by M from above when we use (19). When $\beta > 1$, implying $M < N$, the representation (4) only gives us access to M of N eigenvalues of \hat{S} , which is not sufficient to reconstruct the probability density $p(\lambda)$. In order to access the regime of $\beta > 1$ one needs to find a better approximation to (17) than (19).

Note that the eigenvalue distribution of the matrix \hat{S} has been studied numerically by Akkermans *et al.* in the context of light propagation in atomic gases (see figure 1 of [16]) without proposing any analytical approximation to it. The parameter $\beta \sim N/(k_0L)^2$ has been introduced in that work as a ratio of the number of atoms N to

the number of transverse optical modes $N_{\perp} \propto (k_0 L)^2$. The same parameter appeared in [12, 13, 14, 15] as a superradiant decay rate in a cold atomic gas. Hence the results of this section complement and extend the works [12, 13, 14, 15, 16].

4. Eigenvalue distribution of cosc matrix

Let us now consider an Euclidean random matrix with elements defined using the cardinal cosine (cosc) function:

$$C_{ij} = f(\mathbf{r}_i - \mathbf{r}_j) = (1 - \delta_{ij}) \frac{\cos(k_0 |\mathbf{r}_i - \mathbf{r}_j|)}{k_0 |\mathbf{r}_i - \mathbf{r}_j|} \quad (25)$$

The prefactor $1 - \delta_{ij}$ allows us to deal with the divergence of the function $\cos(x)/x$ for $x \rightarrow 0$. However, in the beginning of our analysis we will ignore this prefactor and will use $C_{ij} = \cos(k_0 |\mathbf{r}_i - \mathbf{r}_j|)/k_0 |\mathbf{r}_i - \mathbf{r}_j|$ for all i, j (the diagonal elements of \hat{C} are thus infinite). Proceeding as in the previous section, we find

$$T_{mn} \simeq \frac{4\pi N}{k_0 V} \frac{1}{q_m^2 - k_0^2} \delta_{mn} \quad (26)$$

under the same approximations as in (18) (i.e., we extended integration over $\Delta \mathbf{r}$ to the whole space). The matrix \hat{T} defined by (26) has infinite size.

The divergence of (26) for $q_m \rightarrow k_0$ can be traced back to the neglecting of the finiteness of the volume V when extending integration over $\Delta \mathbf{r}$ to the whole space. Taking into account the fact that Δr cannot exceed a maximum value of the order of L , the divergence is regularized and the resulting T_{mn} changes sign rapidly but continuously in a strip of width $\sim 1/L$ around $q_m = k_0$. In the following, we will neglect the contribution of \mathbf{q}_m 's inside the spherical shell corresponding to this strip to \hat{C} because (i) the shell has small thickness in the limit of $k_0 L \gg 1$ that we are interested in and (ii) \mathbf{q}_m 's situated symmetrically with respect to the surface $q_m = k_0$ yield contributions of equal magnitude but opposite signs which mutually cancel. More precisely, we will exclude a shell of thickness $2\pi\alpha'/L$ around $q_m = k_0$ and will use (26) outside this shell [see figure 1(b)]. The numerical constant $\alpha' \sim 1$ will be fixed later. The matrix \hat{C} therefore takes the form:

$$\hat{C} = -\hat{H}^{(1)} \hat{T}^{(1)} \hat{H}^{(1)\dagger} + \hat{H}^{(3)} \hat{T}^{(3)} \hat{H}^{(3)\dagger}. \quad (27)$$

Here the first term describes the contribution of $q_m < k_0 - \alpha'\pi/L$ with $T_{mn}^{(1)} = 4\pi N/[k_0 V(k_0^2 - q_m^2)]\delta_{mn}$. The matrix $\hat{T}^{(1)}$ is a diagonal square matrix of size $M_1 \simeq (4\pi/3)(k_0 - \alpha'\pi/L)^3 (L/2\pi)^3$ obtained by dividing the volume of a sphere of radius $k_0 - \alpha'\pi/L$ [region 1 corresponding to the inner sphere in figure 1(b)] by the volume $(2\pi/L)^3$ associated with a single mode. The second term in (27) corresponds to $q_m > k_0 + \alpha'\pi/L$ [region 3 in figure 1(b)]. The matrix $\hat{T}^{(3)}$ is, again, diagonal, with elements $T_{mn}^{(3)} = 4\pi N/[k_0 V(q_m^2 - k_0^2)]\delta_{mn}$ but, in contrast to $\hat{T}^{(1)}$, has infinite size. We will treat this matrix as a finite-size matrix of size $M_3 \simeq (4\pi/3)[q_{\max}^3 - (k_0 + \alpha'\pi/L)^3](L/2\pi)^3$, corresponding to taking into account only $q_m \leq q_{\max}$. The limit of $q_{\max} \rightarrow \infty$ will be

taken at the end. The minus sign in front of the first sign in (27) was introduced to work with a positive-definite matrix $\hat{T}^{(1)}$.

The Green's function of the matrix $\hat{T}^{(1)}$ is

$$\begin{aligned} \mathcal{G}_{\hat{T}^{(1)}}(z) &= \frac{1}{M_1} \text{Tr} \frac{1}{z - \hat{T}^{(1)}} \\ &= \frac{1}{M_1} \sum_{q_m < k_0 - \alpha' \pi / L} \frac{1}{z - \frac{4\pi N}{k_0 V} \frac{1}{k_0^2 - q_m^2}} \\ &\simeq \frac{4\pi N}{M_1 (\rho \lambda_0^3)} \int_0^{1 - \frac{\alpha' \pi}{k_0 L}} d\kappa \kappa^2 \frac{1}{z - \frac{\rho \lambda_0^3}{2\pi^2} \frac{1}{1 - \kappa^2}}, \end{aligned} \quad (28)$$

where the wavelength $\lambda_0 = 2\pi/k_0$ and $\rho \lambda_0^3$ is the average number of points \mathbf{r}_i per wavelength cube. The last line of this equation was obtained in the limit of $k_0 L \gg 1$ by approximately replacing the summation over a set of discrete wavevectors \mathbf{q}_m by an integration over $\boldsymbol{\kappa} = \mathbf{q}_m/k_0$. The integral in (28) can be evaluated yielding

$$\begin{aligned} \mathcal{G}_{\hat{T}^{(1)}}(z) &= \frac{2N}{\pi M_1 z} \left\{ \left(1 - \frac{\alpha' \pi}{k_0 L}\right) \left[\frac{2\pi^2}{3\rho \lambda_0^3} \left(1 - \frac{\alpha' \pi}{k_0 L}\right)^2 - \frac{1}{z} \right] \right. \\ &\quad \left. + \frac{1}{z} \sqrt{\frac{\rho \lambda_0^3}{2\pi^2 z} - 1} \arctan \frac{1 - \frac{\alpha' \pi}{k_0 L}}{\sqrt{\frac{\rho \lambda_0^3}{2\pi^2 z} - 1}} \right\}. \end{aligned} \quad (29)$$

A similar calculation can be performed for the Green's function of $\hat{T}^{(3)}$ except that the integration in (28) extends from $1 + \alpha' \pi/k_0 L$ to κ_{\max} , M_1 is replaced by M_3 , and $1 - \kappa^2$ in the integrand of (28) — by $\kappa^2 - 1$. We find

$$\begin{aligned} \mathcal{G}_{\hat{T}^{(3)}}(z) &= \frac{2N}{\pi M_3 z} \left\{ \left[\kappa_{\max} - \left(1 + \frac{\alpha' \pi}{k_0 L}\right) \right] \left[\frac{2\pi^2}{3\rho \lambda_0^3} (\kappa_{\max}^2 \right. \right. \\ &\quad \left. \left. + \left(1 + \frac{\alpha' \pi}{k_0 L}\right) \left(\kappa_{\max} + 1 + \frac{\alpha' \pi}{k_0 L} \right) \right) + \frac{1}{z} \right] \\ &\quad + \frac{1}{z} \sqrt{-\frac{\rho \lambda_0^3}{2\pi^2 z} - 1} \left[\arctan \frac{1 + \frac{\alpha' \pi}{k_0 L}}{\sqrt{-\frac{\rho \lambda_0^3}{2\pi^2 z} - 1}} \right. \\ &\quad \left. \left. - \arctan \frac{\kappa_{\max}}{\sqrt{-\frac{\rho \lambda_0^3}{2\pi^2 z} - 1}} \right] \right\}. \end{aligned} \quad (30)$$

Because the two terms in (27) correspond to contributions of different parts of \mathbf{q} -space, they are asymptotically free and hence the Blue function of their sum (i.e. of the matrix \hat{C}) can be found as a sum of their Blue functions. The Blue functions of $\hat{H}^{(1)} \hat{T}^{(1)} \hat{H}^{(1)\dagger}$ and $\hat{H}^{(3)} \hat{T}^{(3)} \hat{H}^{(3)\dagger}$ are found using (14), whereas the Blue function of $-\hat{H}^{(1)} \hat{T}^{(1)} \hat{H}^{(1)\dagger}$ is equal to $-B_{\hat{H}^{(1)} \hat{T}^{(1)} \hat{H}^{(1)\dagger}}(-z)$. The Blue function of the sum $\hat{C} = -\hat{H}^{(1)} \hat{T}^{(1)} \hat{H}^{(1)\dagger} + \hat{H}^{(3)} \hat{T}^{(3)} \hat{H}^{(3)\dagger}$ is a sum of individual Blue functions, minus $1/z$:

$$B_{\hat{C}}(z) = -B_{\hat{H}^{(1)} \hat{T}^{(1)} \hat{H}^{(1)\dagger}}(-z) + B_{\hat{H}^{(3)} \hat{T}^{(3)} \hat{H}^{(3)\dagger}}(z) - 1/z$$

$$\begin{aligned}
 &= \frac{1}{z} + \frac{2\kappa_{\max}}{\pi} - \frac{\rho\lambda_0^3}{2\pi^2\beta'} + \frac{2}{\pi} \sqrt{-1 - \frac{\rho\lambda_0^3}{2\pi^2}z} \\
 &\times \left[\arctan \frac{1 + \frac{\rho\lambda_0^3}{8\pi\beta'}}{\sqrt{-1 - \frac{\rho\lambda_0^3}{2\pi^2}z}} - \arctan \frac{1 - \frac{\rho\lambda_0^3}{8\pi\beta'}}{\sqrt{-1 - \frac{\rho\lambda_0^3}{2\pi^2}z}} \right. \\
 &\left. - \arctan \frac{\kappa_{\max}}{\sqrt{-1 - \frac{\rho\lambda_0^3}{2\pi^2}z}} \right]. \tag{31}
 \end{aligned}$$

where $\beta' = \pi N/\alpha'(k_0L)^2$.

The final step consists in taking the limit $\kappa_{\max} \rightarrow \infty$. We now recall that up to now we ignored the fact that the matrix \hat{C} had zero diagonal elements $C_{ii} = 0$. Instead, we considered a matrix with infinitely large diagonal elements. Such a matrix naturally has infinite eigenvalues and to go back to the case of $C_{ii} = 0$ we have to shift the eigenvalues to the left. To determine the exact shift, we compute the average of λ from (31) using (12) and subtract it from (31) because we know that for the matrix \hat{C} defined by (25), $\langle \lambda \rangle = (1/N)\langle \text{Tr} \hat{C} \rangle = 0$ exactly. We then compute the second moment $\langle \lambda^2 \rangle$ and require that its value in the limit of $\rho\lambda_0^3/\beta' \propto 1/k_0L \rightarrow 0$ is equal to β defined by (24). This fixes $\beta' = (\pi^2/4)\beta$ corresponding to $\alpha' \simeq 0.45$. The final expression for the Blue function of \hat{C} is

$$\begin{aligned}
 B_{\hat{C}}(z) &= \frac{1}{z} - \frac{2}{\pi} \text{arccoth} \frac{4\pi^3\beta}{\rho\lambda_0^3} + \frac{2}{\pi} \sqrt{-1 - \frac{\rho\lambda_0^3}{2\pi^2}z} \\
 &\times \left[\arctan \frac{1 + \frac{\rho\lambda_0^3}{2\pi^3\beta}}{\sqrt{-1 - \frac{\rho\lambda_0^3}{2\pi^2}z}} - \arctan \frac{1 - \frac{\rho\lambda_0^3}{2\pi^3\beta}}{\sqrt{-1 - \frac{\rho\lambda_0^3}{2\pi^2}z}} - \frac{\pi}{2} \right]. \tag{32}
 \end{aligned}$$

The Green's function $\mathcal{G}_{\hat{C}}(z)$ can be found from this equation by solving $B_{\hat{C}}[\mathcal{G}(z)] = z$ which, for the general case, we do numerically.

Let us consider the low-density limit of (32), $\rho\lambda_0^3 \ll 1$. For large box size $L \gg 1/k_0$ the arguments of arctan functions in (32) are close to $-i$. They can be thus expanded in series in the vicinity of this point. In the resulting expression we take the limits of $\rho\lambda_0^3 \rightarrow 0$ and $\rho\lambda_0^3/\beta \sim 1/k_0L \rightarrow 0$ to obtain

$$B_{\hat{C}}(z) = \frac{1}{z} - \frac{1}{\pi} \ln \frac{1 - \frac{\pi}{2}\beta z}{1 + \frac{\pi}{2}\beta z}, \quad \rho\lambda_0^3 \ll 1. \tag{33}$$

This expression has two important limits. For $\beta \ll 1$ we find $B_{\hat{C}}(z) = \beta z + 1/z$ which is the Blue function of the Wigner semi-circle law $p(\lambda) = \sqrt{4\beta - \lambda^2}/2\pi\beta$. In the opposite limit of $\beta \gg 1$ we have $B_{\hat{C}}(z) = -i + 1/z$, which corresponds to the Cauchy distribution $p(\lambda) = 1/[\pi(1 + \lambda^2)]$. Equation (33) therefore describes a transition from the Wigner semi-circle law at $\beta \ll 1$ to the Cauchy distribution at $\beta \rightarrow \infty$. The eigenvalue distribution following from (33) is always symmetric with respect to $\lambda = 0$ and vanishes for $|\lambda| > \lambda_*$ (see the left panel of figure 3). The latter can be found by

|| Subtracting a constant from the Blue function $B(z)$ results in shifting the eigenvalue distribution $p(\lambda)$.

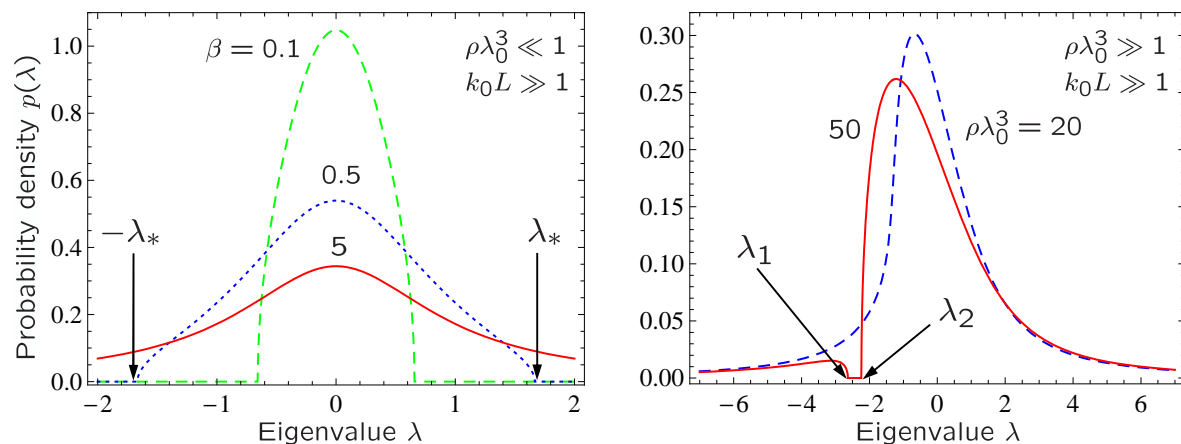


Figure 3. Probability density of eigenvalues of a square $N \times N$ Euclidean matrix \hat{C} with elements $C_{ij} = (1 - \delta_{ij}) \cos(k_0 |\mathbf{r}_i - \mathbf{r}_j|) / k_0 |\mathbf{r}_i - \mathbf{r}_j|$, where the N points \mathbf{r}_i are randomly chosen inside a 3D cube of side L . The left panel corresponds to the low-density limit and is obtained using (33) with $\beta = 0.1, 0.5$ and 5 . The distributions are symmetric and vanish for $|\lambda| > \lambda_*$ with λ_* given by (34). The right panel illustrates our equation (35) obtained in the high-density limit for two densities $\rho\lambda_0^3 = 20$ and 50 . For $\rho\lambda_0^3 > 30.3905$ the distribution develops a gap in between λ_1 and λ_2 given by (36) and (37), respectively.

using the relation $p(\lambda) \propto \text{Im}\mathcal{G}(z = \lambda + i\epsilon)$ and the link between $\mathcal{G}(z)$ and $B(z)$. Simple reasoning shows that the boundary λ_* of the domain of existence of eigenvalues is the solution of equation $B'_{\hat{C}}(z) = 0$ [25]:

$$\lambda_* = \sqrt{\beta \left(1 + \frac{\pi^2}{4}\beta\right)} + \frac{2}{\pi} \text{arccoth} \sqrt{1 + \frac{4}{\pi^2}\beta}. \quad (34)$$

This equation simplifies to $\lambda_* = 2\sqrt{\beta}$ for $\beta \ll 1$ and to $\lambda_* = \frac{\pi}{2}\beta$ for $\beta \gg 1$.

Another important limit of (32) is that of high density $\rho\lambda_0^3 \gg 1$ of points in a large box $L \gg 1/k_0$. In this limit the arguments of arctan functions in (32) are small and we can put $\arctan x \simeq x$. Taking the limit of $\rho\lambda_0^3/\beta' \sim 1/k_0 L \rightarrow 0$ we then obtain

$$B_{\hat{C}}(z) = \frac{1}{z} + i\sqrt{1 + \frac{\rho\lambda_0^3}{2\pi^2}z}, \quad \rho\lambda_0^3 \gg 1. \quad (35)$$

For $\rho\lambda_0^3$ below a critical value $(\rho\lambda_0^3)_c = 30.3905$ the eigenvalue distribution corresponding to (35) is asymmetric but bell-shaped, similarly to the case of low density. For $\rho\lambda_0^3 > (\rho\lambda_0^3)_c$, however, the distribution develops a gap: $p(\lambda) = 0$ for $\lambda_1 < \lambda < \lambda_2$, where $\lambda_{1,2} = B_{\hat{C}}(z_{1,2})$ with $z_{1,2}$ being solutions of $B'_{\hat{C}}(z) = 0$ (see the right panel of figure 3). In the limit of $\rho\lambda_0^3 \gg (\rho\lambda_0^3)_c$ we have

$$\lambda_1 \simeq -\frac{\rho\lambda_0^3}{2\pi^2} - \frac{\pi^2}{2\rho\lambda_0^3}, \quad (36)$$

$$\lambda_2 \simeq -\frac{3}{2\pi^{2/3}}(\rho\lambda_0^3)^{1/3} + \frac{\pi^{2/3}}{2(\rho\lambda_0^3)^{1/3}} + \frac{\pi^2}{6\rho\lambda_0^3}. \quad (37)$$

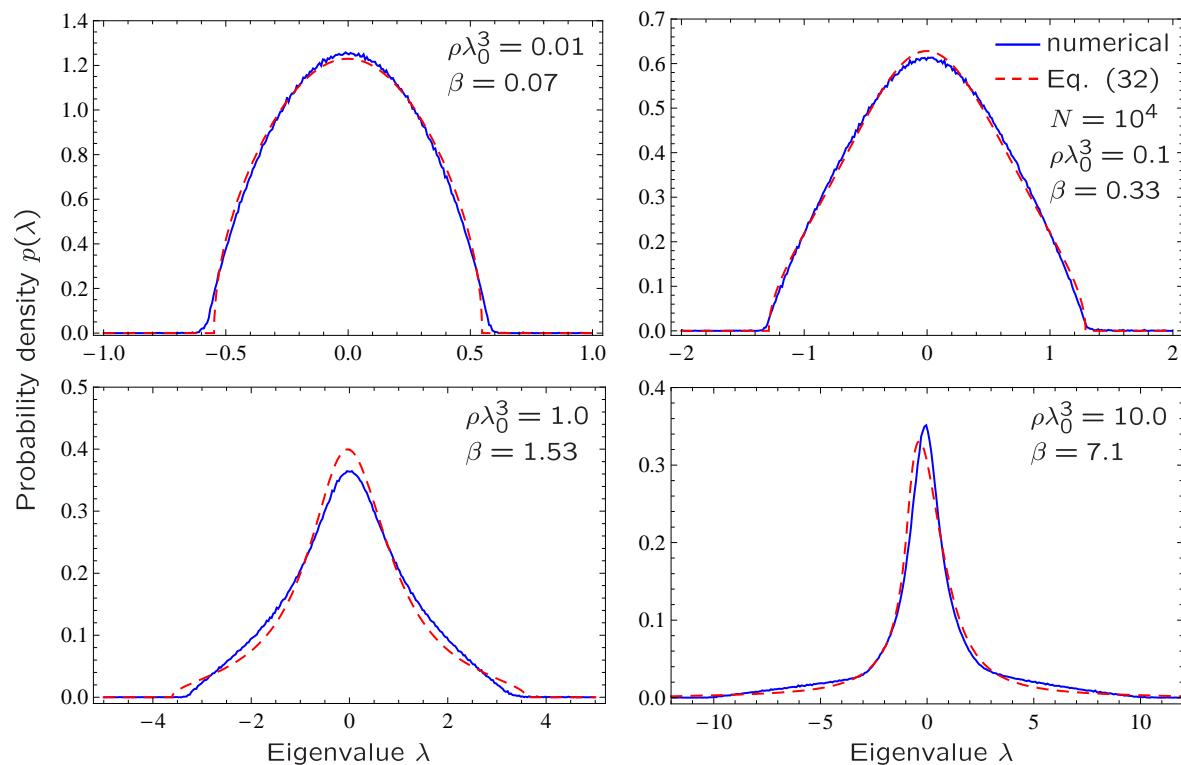


Figure 4. Probability density of eigenvalues of a square $N \times N$ Euclidean matrix \hat{C} with elements $C_{ij} = (1 - \delta_{ij}) \cos(k_0 |\mathbf{r}_i - \mathbf{r}_j|) / k_0 |\mathbf{r}_i - \mathbf{r}_j|$, where the N points \mathbf{r}_i are randomly chosen inside a 3D cube of side L . Numerical results (blue solid lines) obtained for $N = 10^4$ after averaging over 10 realizations are compared to our equation (32) (red dashed lines) with $\beta = 2.8N / (k_0 L)^2$ for several densities ρ of points ($\lambda_0 = 2\pi / k_0$).

In figure 4 we compare $p(\lambda)$ following from (32) with the results of numerical simulations. We find the Green's function $\mathcal{G}_{\hat{C}}(z)$ by solving the equation $B_{\hat{C}}[\mathcal{G}_{\hat{C}}(z)] = z$ numerically and then evaluate the probability distribution of eigenvalues $p(\lambda)$ with the help of (10). When $\beta \rightarrow 0$, the distribution $p(\lambda)$ tends to the Wigner semi-circle law. In contrast, for large $\beta > 1$ it resembles a Cauchy distribution. A good agreement between numerical results and (32) is observed not only for $\beta < 1$ (similarly to the case of sinc matrix in section 3) but for $\beta > 1$ as well. Note that in contrast to the Marchenko-Pastur law (21) parameterized by a single parameter β , the Green's function (32) and the corresponding probability distribution depend on two parameters β and $\rho\lambda_0^3$. A good agreement between (32) and numerical simulations is obtained at low densities $\rho\lambda_0^3 < 30$ (see figure 4). In contrast, at higher densities $\rho\lambda_0^3 \gtrsim 30$ (not shown) the probability distribution following from (32) develops a gap that is not present in numerical results. Interestingly, this gap in the probability distribution appears at the same density $\rho\lambda_0^3 \approx 30$ for all β .

5. Eigenvalue distribution of $\text{cosc} + i \text{sinc}$ matrix

The matrices \hat{C} and \hat{S} can be combined in a single complex non-Hermitian matrix: $\hat{C} + i(\hat{S} - \hat{\mathbb{I}})$, with $\hat{\mathbb{I}}$ the identity matrix. The theory of free random variables [22] allows one to study the statistical distribution of the complex eigenvalues of this matrix based on the properties of the matrices \hat{C} and \hat{S} that we considered in the previous sections [29]. This, however, requires asymptotic freeness of \hat{C} and \hat{S} . Unfortunately, the matrices \hat{S} and \hat{C} defined by (16) and (25) through *the same* set of points $\{\mathbf{r}_i\}$ turn out to be not asymptotically free, except in the limit of $\beta \rightarrow 0$ and $\rho\lambda_0^3 \rightarrow 0$ (see section 6). We therefore start our study of non-Hermitian Euclidean random matrices by the case of a matrix $\hat{X} = \hat{C} + i(\hat{S}' - \hat{\mathbb{I}})$, where *two different and independent* sets of points $\{\mathbf{r}_i\}$ and $\{\mathbf{r}'_i\}$ are used to define the real and imaginary parts of \hat{X} :

$$\begin{aligned} C_{ij} &= (1 - \delta_{ij}) \frac{\cos(k_0|\mathbf{r}_i - \mathbf{r}_j|)}{k_0|\mathbf{r}_i - \mathbf{r}_j|}, \\ S'_{ij} &= \frac{\sin(k_0|\mathbf{r}'_i - \mathbf{r}'_j|)}{k_0|\mathbf{r}'_i - \mathbf{r}'_j|}. \end{aligned} \quad (38)$$

The matrix \hat{X} defined in this way is similar to the matrix \hat{G} defined in the introduction except that it has no correlation between its real and imaginary parts. As we will see from the following, these correlations become important for $\beta > 1$. One can easily show that for the same reason as the one that ensured positiveness of the eigenvalues of the matrix \hat{S} in section 3, the complex eigenvalues λ of the matrix \hat{X} obey $\text{Im}\lambda > -1$.

For non-Hermitian matrices, the Green's function loses its analyticity inside two-dimensional domains ('islands') on the complex plane, instead of segments of the real axis in the Hermitian case. In [29] Jarosz and Nowak provide a simple algorithm, based on the algebra of quaternions, to calculate the non-holomorphic Green's function $\mathcal{G}_{\hat{X}}(z)$ and the correlator of left $|L_i\rangle$ and right $|R_i\rangle$ eigenvectors [30] $\mathcal{C}_{\hat{X}}(z) = -(\pi/N) \sum_{i=1}^N \langle L_i|L_i\rangle \langle R_i|R_i\rangle \delta(z - \lambda_i)$ inside these domains for any non-Hermitian matrix of the form $\hat{X} = \hat{H}_1 + i\hat{H}_2$, where \hat{H}_1 and \hat{H}_2 are two asymptotically free Hermitian matrices with known Blue functions. In our case, $\hat{H}_1 = \hat{C}$ and $\hat{H}_2 = \hat{S}' - \hat{\mathbb{I}}$. In the limit of $\beta \ll 1$ the Blue functions are $B_1(z) = \beta z + 1/z$ (section 4) and $B_2(z) = 1/(1 - \beta z) - 1 + 1/z$ (section 3). $\mathcal{G}_{\hat{X}}(z)$ and $\mathcal{C}_{\hat{X}}(z)$ can be then found analytically:

$$\mathcal{G}_{\hat{X}}(z = x + iy) = \frac{x}{2\beta} - \frac{i}{2} \left[\frac{y}{\beta(1+y)} + \frac{1}{2+y} \right], \quad (39)$$

$$\begin{aligned} \mathcal{C}_{\hat{X}}(z = x + iy) &= \left(\frac{x}{2\beta} \right)^2 + \frac{1}{4} \left[\frac{y}{\beta(1+y)} - \frac{1}{2+y} \right]^2 \\ &\quad - \frac{1}{\beta(1+y)(2+y)}. \end{aligned} \quad (40)$$

The correlator (40) must vanish on the borderline of the eigenvalue domains. We therefore readily obtain an equation for the borderline of the domain of existence of

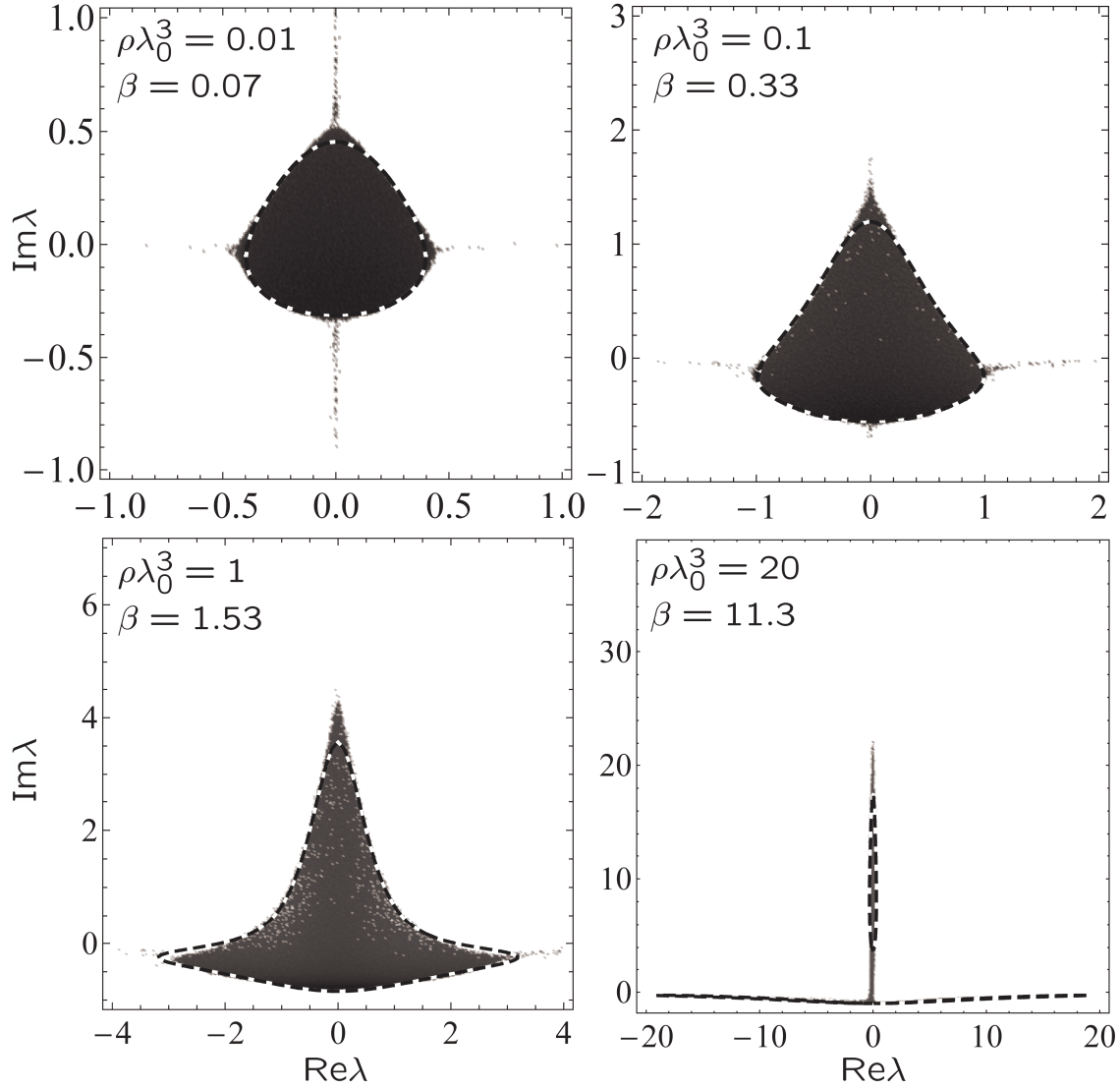


Figure 5. Density plot of the logarithm of the probability density of eigenvalues λ of a square $N \times N$ Euclidean matrix \hat{X} with elements $X_{ij} = (1 - \delta_{ij})[\cos(k_0|\mathbf{r}_i - \mathbf{r}_j|)/k_0|\mathbf{r}_i - \mathbf{r}_j| + i \sin(k_0|\mathbf{r}_i - \mathbf{r}_j|)/k_0|\mathbf{r}_i - \mathbf{r}_j|]$ at 4 different densities ρ of points $\mathbf{r}_i, \mathbf{r}'_i$ per wavelength $\lambda_0 = 2\pi/k_0$ cube. $2N = 2 \times 10^4$ points \mathbf{r}_i and \mathbf{r}'_i ($i = 1, \dots, N$) are randomly chosen inside a 3D cube; the probability distributions are estimated from 10 realizations of $\{\mathbf{r}_i\}$ and $\{\mathbf{r}'_i\}$. Dashed lines show the domain of existence of eigenvalues following from the free probability theory.

eigenvalues of \hat{X} on the complex plane:

$$x^2 + \left(\frac{y}{1+y} - \frac{\beta}{2+y} \right)^2 - \frac{4\beta}{(1+y)(2+y)} = 0, \quad (41)$$

where $x = \text{Re}\lambda$ and $y = \text{Im}\lambda$. The probability density inside this domain is

$$\begin{aligned} p(x, y) &= \frac{1}{2\pi} [\partial_x \text{Re} \mathcal{G}_{\hat{X}}(x, y) - \partial_y \text{Im} \mathcal{G}_{\hat{X}}(x, y)] \\ &= \frac{1}{4\pi} \left[\frac{1}{\beta} + \frac{1}{\beta(1+y)^2} - \frac{1}{(2+y)^2} \right]. \end{aligned} \quad (42)$$

A better model for the Blue function of the matrix \hat{C} is (33). If we use this equation instead of $B_1(z) = \beta z + 1/z$ above, analytic calculation becomes impossible but we can still compute $\mathcal{G}_{\hat{X}}(z)$ and $\mathcal{C}_{\hat{X}}(z)$ numerically. The resulting borderline of the eigenvalue domain is shown in figure 5 (dashed lines) together with the eigenvalue distribution of the matrix $\hat{X} = \hat{C} + i(\hat{S}' - \hat{\mathbb{I}})$ found by the numerical diagonalization of a set of $10^4 \times 10^4$ random matrices. At the smallest density considered $\rho\lambda_0^3 = 0.01$, the borderline found using (33) is very close to (41). At higher densities the former describes numerical results much better than (41).

Equation (41) predicts a splitting of the eigenvalue domain in two parts at $\beta = 8$. The more accurate calculation using (33) makes a similar prediction (see the lower right panel of figure 5). However, the eigenvalues of the matrix \hat{X} do not show such a splitting and form an ‘inverted T’ distribution on the complex plane instead. This is due to the fact that the Marchenko-Pastur law (21) fails to describe the eigenvalue distribution of the matrix \hat{S}' at $\beta > 1$ and hence the Blue function $1/(1 - \beta z) + 1/z$ that we assumed for \hat{S}' is not a good approximation anymore.

It is worthwhile to note that large random non-Hermitian matrices similar to our matrix \hat{X} were considered previously by Haake *et al.* [32] (with the help of the replica trick), Lehmann *et al.* [33] (using the supersymmetry method) and Janik *et al.* [26] (using the free probability theory). These authors studied matrices of the form $\hat{H} + ic\hat{\Gamma}$, where \hat{H} was an Hermitian matrix with random elements obeying Gaussian statistics, $\hat{\Gamma}$ was a Wishart random matrix [i.e. a matrix of the form (20)], and c was a real number controlling the ‘degree of non-Hermiticity’ of the matrix. The splitting of the domain of existence of eigenvalues in two parts was observed when c was increased. This is different from our matrix \hat{X} that has elements with equal variances β/N of real and imaginary parts (hence always the same degree of non-Hermiticity) but that still exhibits the splitting of the eigenvalue domain when β is increased.

6. Eigenvalue distribution of the complex expc matrix

By analogy with the cardinal sine and cosine functions, a ‘cardinal complex exponent’ function can be defined as $f(x) = \exp(ix)/x$. The Euclidean random matrix \hat{G} corresponding to this function has elements

$$G_{ij} = f(\mathbf{r}_i - \mathbf{r}_j) = (1 - \delta_{ij}) \frac{\exp(ik_0|\mathbf{r}_i - \mathbf{r}_j|)}{k_0|\mathbf{r}_i - \mathbf{r}_j|}. \quad (43)$$

This matrix has a particular importance in the problem of wave scattering by an ensemble of N point-like scatterers: indeed, as we noted already in the introduction, each element of the matrix \hat{G} is a Green’s function of the scalar Helmholtz equation (1).

Although the matrix \hat{G} is similar to the matrix \hat{X} considered in the previous section, the analytic study of its properties is much more involved. On the one hand, similarly to the eigenvalues of \hat{X} , the eigenvalues of \hat{G} obey $\text{Im}\lambda > -1$. On the other hand, correlations that arise between the real and imaginary parts of \hat{G} due to the presence of the same set of points $\{\mathbf{r}_i\}$ in both $\text{Re}\hat{G} = \hat{C}$ and $\text{Im}\hat{G} = \hat{S}' - \hat{\mathbb{I}}$ preclude the use of the free

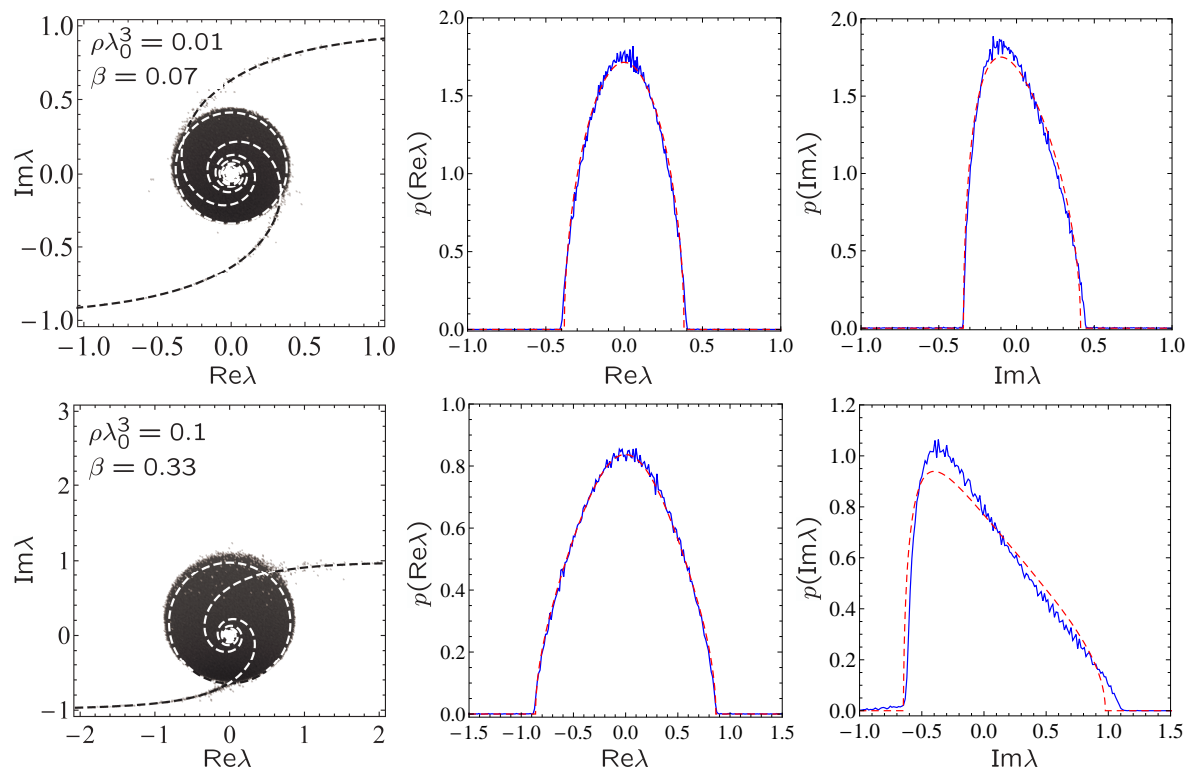


Figure 6. Left column: density plot of the logarithm of the probability density of eigenvalues λ of a square $N \times N$ Euclidean matrix \hat{G} with elements $G_{ij} = (1 - \delta_{ij}) \exp(ik_0|\mathbf{r}_i - \mathbf{r}_j|)/k_0|\mathbf{r}_i - \mathbf{r}_j|$ at low densities $\rho\lambda_0^3 = 0.01$ (first row) and 0.1 (second row), $\lambda_0 = 2\pi/k_0$. $N = 10^4$ points \mathbf{r}_i are randomly chosen inside a 3D cube. Dashed circles are centered at $(0, \frac{1}{2}\beta)$ and have radii $\sqrt{2\beta}$. Eigenvalues of a 2×2 matrix would lie on dashed spirals. Central column: marginal probability density of the real part of λ compared to our equation (32) with β replaced by $\frac{1}{2}\beta$ (dashed red line). Right column: marginal probability density of the imaginary part of λ compared to the Marchenko-Pastur law (21) with λ replaced by $\text{Im}\lambda + 1$ and β replaced by $\frac{1}{2}\beta$ (dashed red line).

probability approach described in section 5. Another way to deal with non-Hermitian matrices is to double the size of the space and to manipulate Hermitian matrices of size $2N \times 2N$ (in the ‘quaternion’ space [26] or in the ‘chiral’ space [27]). Due to technical difficulties, however, this approach can be put in practice only in certain special cases like, e.g., the case of circularly invariant distributions $p(\lambda) = p(|\lambda|)$ [28]. It turns out, however, that in the limit of β , $\rho\lambda_0^3 \rightarrow 0$, the matrices \hat{C} and \hat{S} obey the conditions of asymptotic freeness. In this limit, we can therefore apply the results of section 5 to the matrix \hat{G} .

In the limit of $\beta \rightarrow 0$, (41) is approximately a circle on the complex plane. The radius of this circle is $\sqrt{2\beta}$ and the position of the center is $x_0 = 0$, $y_0 = \frac{1}{2}\beta$ as can be seen from (41) by assuming $y \ll 1$ in the denominators. To derive this result in a more rigorous way, we substitute the equation of a circle, $x = r\sqrt{2\beta} \cos \phi$ and $y = r\sqrt{2\beta} \sin \phi + \frac{1}{2}\beta$, in (41). The l.h.s. of the resulting equation is then expanded

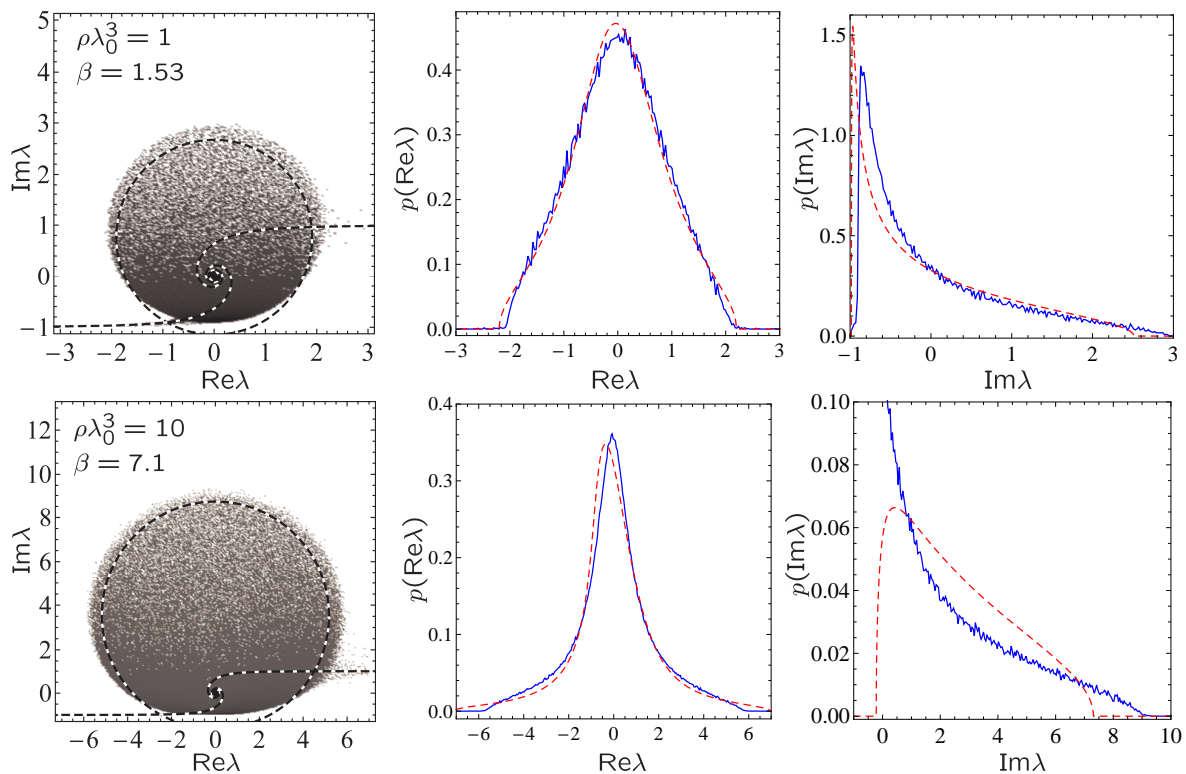


Figure 7. Same as figure 6 but for intermediate densities $\rho\lambda_0^3 = 1$ (first row) and 10 (second row). Dashed circles are centered at $(0, \frac{1}{2}\beta)$ and have radii R given by (44).

in orders of β and coefficients c_ν in front of consecutive powers of β are analyzed. The coefficient c_0 in front of β^0 is zero whatever r and h . The coefficient in front of β^1 is $c_1 = 2(r^2 - 1)$. Equation (41) is therefore obeyed up to linear order in β for $r = 1$ and any h . The next term is of the order $\beta^{3/2}$ and it cannot be put to zero simply by adjusting h because $c_{3/2}$ depends on ϕ : $c_{3/2}(\phi) = \sqrt{2} \sin \phi (h + 2 \cos 2\phi)$. We thus search for h that minimizes the integral $\int_0^{2\pi} d\phi c_{3/2}^2(\phi) = 2\pi(h^2 - 2h + 2)$. This yields $h = 1$. As we show in figure 6, a circle of radius $\sqrt{2\beta}$ centered at $(0, \frac{1}{2}\beta)$ is indeed a good approximation to the domain of existence of eigenvalues of the matrix \hat{G} for small β and $\rho\lambda_0^3$. The density of eigenvalues inside the circle is not homogeneous: expanding (42) around $y = y_0$ and taking the limit $\beta \rightarrow 0$ we obtain $p(x, y) \simeq (1 - y)/2\pi\beta$. In addition to the eigenvalues inside the circle, there exist eigenvalues that follow the spirals corresponding to the eigenvalues G_{12} and $-G_{12}$ of a 2×2 matrix \hat{G} . Interestingly, the spirals are quite robust and survive at all densities (see figure 6, figure 7 and figure 8).

Because the matrices \hat{S} and \hat{C} studied in previous sections represent the imaginary and real parts of the matrix \hat{G} , respectively, one might expect some links between the probability distributions of eigenvalues of \hat{S} and \hat{C} and the marginal probability distributions of the real and imaginary parts of the eigenvalues of \hat{G} . And indeed, we see from the central and right columns of figure 6 that the marginal probability distributions $p(\text{Re}\lambda)$ and $p(\text{Im}\lambda)$ are nicely described by (32) and (21), respectively,

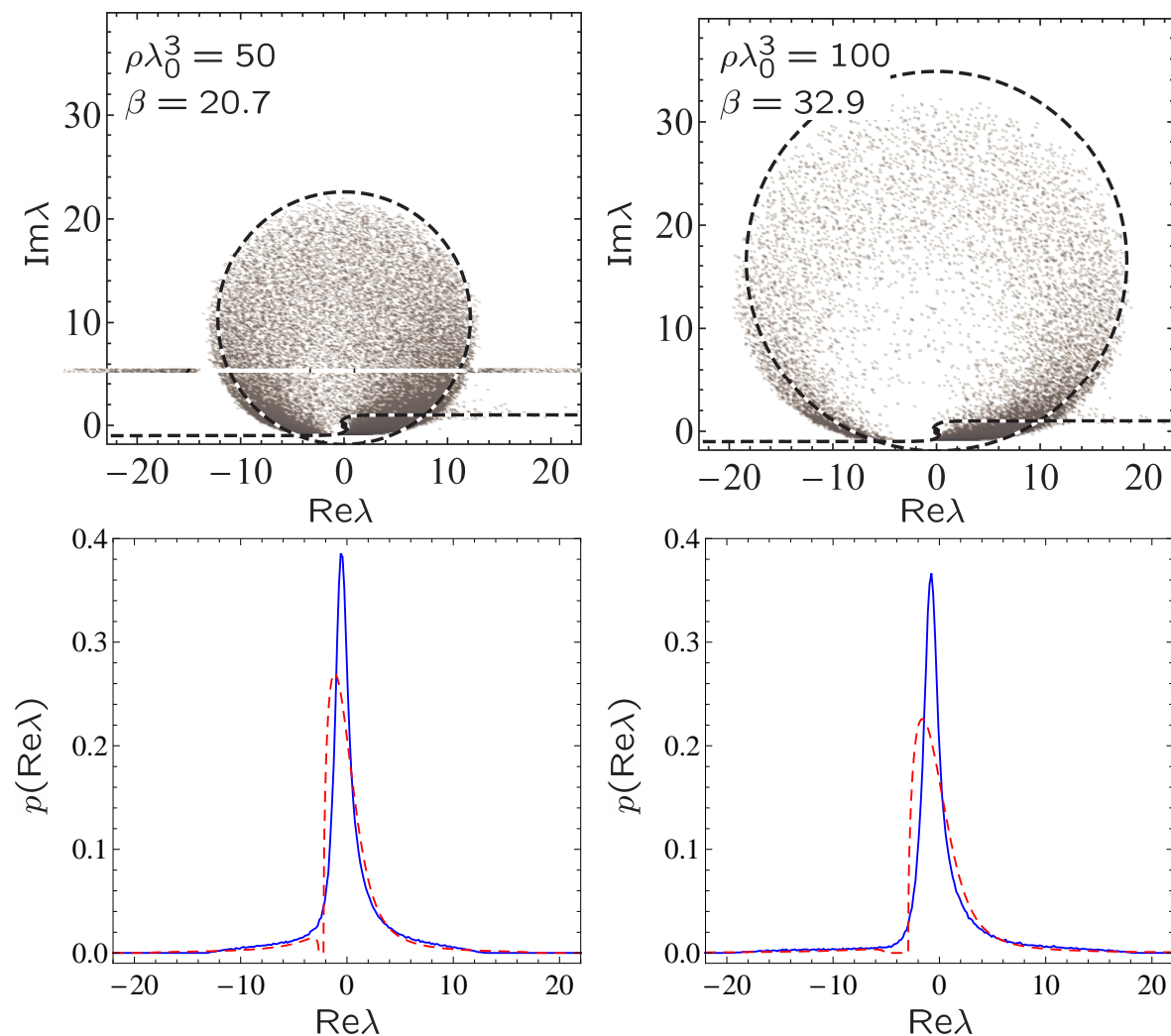


Figure 8. Same as figure 6 and figure 7 but for high densities $\rho\lambda_0^3 = 50$ (left column) and 100 (right column); dashed circles as in figure 7. Note a hole that develops on the left from $\text{Re}\lambda = 0$ near the real axis and the corresponding gap in the marginal distributions of $\text{Re}\lambda$ (dashed red lines). Marginal distributions of $\text{Im}\lambda$ are not shown.

with β replaced by $\frac{1}{2}\beta$. This suggests an interesting interpretation of the Marchenko-Pastur law (21): it can be seen as a projection of a two-dimensional distribution $p(x, y)$ of complex eigenvalues $x + iy$ on the imaginary axis y , provided that $p(x, y)$ is different from zero only inside a circle of radius $2\sqrt{\beta}$ centered at $(0, \beta)$ and that $p(x, y) \propto 1/y$ inside the circle. $p(x, y)$ being independent of x and decaying monotonically with y is consistent with the result that we obtained from the free random variable theory in the limit of $\beta, \rho\lambda_0^3 \rightarrow 0$.

When we increase β but keep the density relatively low ($\rho\lambda_0^3 < 30$, see below), the cloud of eigenvalues grows but keeps its circular shape (see figure 7) ¶. The distribution

¶ Because we present results at a fixed $N = 10^4$, increasing β is achieved by increasing the density $\rho\lambda_0^3$. However, by repeating the analysis at $N = 10^3$ and $N = 5 \times 10^3$ we checked that the distributions

of eigenvalues acquires an important asymmetry: the eigenvalues are ‘attracted’ by the axis $\text{Im}\lambda = -1$. Interestingly, whereas the Marchenko-Pastur law ceases to describe the marginal distribution of $\text{Im}\lambda$ when $\frac{1}{2}\beta$ becomes larger than unity, the region of validity of (32) for the distribution of $\text{Re}\lambda$ is wider: as we show in figure 7, (32) continues to yield reasonable results even for $\frac{1}{2}\beta > 1$. As can be seen from figure 7, even at $\frac{1}{2}\beta \gtrsim 1$ the borderline of the eigenvalues’ domain is still roughly a circle. More accurate inspection reveals that this circle is still centered at $(0, \frac{1}{2}\beta)$ even for $\beta \gg 1$. It touches the line $\text{Im}\lambda = -1$ that it cannot cross. Its radius is, therefore, roughly $\frac{1}{2}\beta$ and not $\sqrt{2\beta}$ as in the limit of small β . To extrapolate between the limits of small and large β we propose the following empirical expression for the radius R of the eigenvalue domain:

$$R^2 \approx 2\beta + \left(\frac{\beta}{2}\right)^2. \quad (44)$$

For $\beta \ll 1$, the second term of this equation is negligible and we recover $R = \sqrt{2\beta}$. For the parameters of figure 6, for example, a circle of radius R given by (44) is virtually indistinguishable from the circle of radius $\sqrt{2\beta}$ shown in the figure. At larger β the second term in (44) starts to play a role and dominates for $\beta \gg 1$. As we show in figure 7, (44) gives a good idea of the part of the complex plane where the eigenvalues of the matrix \hat{G} are concentrated.

At high densities $\rho\lambda_0^3 \gtrsim 30$, a ‘hole’ appears in the eigenvalue distribution that otherwise still preserves its overall circular structure (see figure 8)⁺. Interesting enough, this hole is not accompanied by any visible signatures in the marginal distributions $p(\text{Re}\lambda)$ and $p(\text{Im}\lambda)$. However, the analytic result (32) develops a gap precisely at the same density $\rho\lambda_0^3 \approx 30$ and at the same position at which the hole appears on the complex plane. This suggests that even though (32) does not provide a correct description of the marginal distribution $p(\text{Re}\lambda)$ at such high densities, it still reflects some relevant properties of the distribution of complex eigenvalues λ . Note that at high densities $\rho\lambda_0^3$ the eigenvalue distribution is concentrated near the axis $\text{Im}\lambda = -1$ and the parts of the distribution corresponding to $\text{Im}\lambda \gg 1$ in figure 8 are visible only thanks to the logarithmic scale of the plot.

Finally, we study the marginal distribution of $\text{Im}\lambda$. It has been given special attention previously because, under certain assumptions, it was shown to give the distribution of ‘decay rates’ of quasi-modes in an open random medium [9]. When $\frac{1}{2}\beta > 1$, $p(\text{Im}\lambda + 1)$ does not follow the Marchenko-Pastur law anymore (see figure 7). Based on the results of numerical simulations, Pinheiro *et al.* [9] claimed that at high densities $\rho\lambda_0^3$ the marginal distribution $p(\text{Im}\lambda + 1)$ exhibits a universal $1/x$ decay. Our analysis summarized in figure 9 (left) confirms that such a decay is present, even though it seems to speed up slightly when the density is increased. It turns out that in certain applications of random matrix theory to wave propagation in random media and, in particular, in problems related to random lasing, a special role is played by

presented in figure 7 change only slightly when N and $\rho\lambda_0^3$ are varied to keep β constant.

⁺ By repeating calculations with $N = 10^3$ and $N = 5 \times 10^3$ we found that the appearance of the hole in the eigenvalue distribution is independent of β .

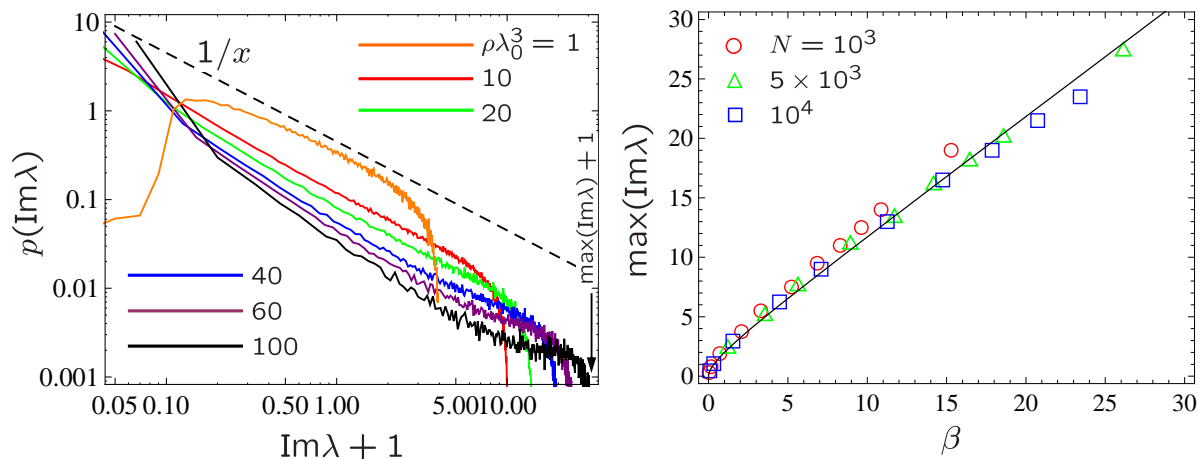


Figure 9. Left: marginal distributions of the imaginary part of the eigenvalues of the matrix \hat{G} computed numerically at densities $\rho\lambda_0^3 = 1, 10, 20, 40, 60$ and 100 (curves from top to bottom) for $N = 10^4$ are compared with the asymptotic law $1/x$ shown by the dashed line. The vertical arrow shows the maximum value of $\text{Im}\lambda$ at which the distribution corresponding to $\rho\lambda_0^3 = 100$ vanishes. Right: $\max(\text{Im}\lambda)$ is shown as a function of β for three different values of N (symbols). At each N , different values of β are obtained by changing the density $\rho\lambda_0^3$ from 0.01 to 100 . The size of the symbols reflects the typical uncertainty in the estimation of $\max(\text{Im}\lambda)$ from numerical data. The solid line shows $\max(\text{Im}\lambda) = \frac{1}{2}\beta + R$ with R given by (44).

the eigenvalues of \hat{G} that have the largest imaginary part [18]. $\max(\text{Im}\lambda)$ is a random number with a probability distribution which is strongly peaked around the point where the distribution $p(\text{Im}\lambda)$ vanishes (see the left panel of figure 9). We show this point in the right panel of figure 9 as a function of β . We have shown that the distribution of complex eigenvalues λ of the matrix \hat{G} occupies a circular domain of radius R given by (44), centered at $\frac{1}{2}\beta$. It follows then that $\max(\text{Im}\lambda) \approx \frac{1}{2}\beta + R$. And indeed, this approximate expression describes numerical results quite reasonably (see the solid line in the right panel of figure 9).

7. Conclusion

In this work we studied eigenvalue distributions of certain Euclidean random matrices that appear in the context of wave propagation in random media. In particular, we considered large $N \times N$ real symmetric matrices \hat{S} and \hat{C} with elements $S_{ij} = \sin(k_0|\mathbf{r}_i - \mathbf{r}_j|)/k_0|\mathbf{r}_i - \mathbf{r}_j|$ and $C_{ij} = (1 - \delta_{ij}) \cos(k_0|\mathbf{r}_i - \mathbf{r}_j|)/k_0|\mathbf{r}_i - \mathbf{r}_j|$, respectively, as well as the non-Hermitian matrix $\hat{G} = \hat{C} + i(\hat{S} - \hat{\mathbb{I}})$. N points \mathbf{r}_i were chosen randomly in a three-dimensional cube of side L with density $\rho = N/L^3$. For the three random matrices under study, the two important parameters of the eigenvalue distributions $p(\lambda)$ are $\beta = 2.8N/(k_0L)^2$ and the number of points per wavelength cube $\rho\lambda_0^3$. β is equal to the variance of eigenvalues λ of both \hat{S} and \hat{C} in the limit of $k_0L \rightarrow \infty$.

In the low-density limit $\rho\lambda_0^3 \ll 1$ and for $\beta < 1$, the distributions of eigenvalues

of Hermitian matrices \hat{S} and \hat{C} are parameterized uniquely by β : the distribution of eigenvalues of \hat{S} is given by the Marchenko-Pastur law (21), whereas the distribution of eigenvalues of \hat{C} can be deduced from the Blue function (33) that we derived in this paper. For $\beta > 1$ the Marchenko-Pastur does not apply to \hat{S} anymore, but our equation (33) still works for \hat{C} as long as $\rho\lambda_0^3$ is small enough. As β increases, (33) describes a transition from the Wigner semi-circle law (at $\beta \ll 1$) to the Cauchy distribution (at $\beta \gg 1$). At high densities $\rho\lambda_0^3 > 1$ the more complete expression (32) that we derived for the Blue function of the matrix \hat{C} applies. It is in good agreement with numerical simulations until $\rho\lambda_0^3 \approx 30$ where it predicts the appearance of a gap in $p(\lambda)$, which is not observed in the numerical data.

The eigenvalue distribution of the non-Hermitian matrix \hat{G} has a circular structure on the complex plane. At small $\beta \ll 1$, the eigenvalues are confined to a circle of radius $\sqrt{2\beta}$ centered at $(0, \frac{1}{2}\beta)$. We obtained this result by combining the results for \hat{S} and \hat{C} in the framework of the theory of free random variables. At larger β , the distribution becomes strongly asymmetric, with much stronger weight of eigenvalues with imaginary parts close to -1 . Our numerical results show that the domain of existence of eigenvalues is still approximately a circle centered at $(0, \frac{1}{2}\beta)$. We proposed an empirical expression for its radius $R^2 \approx 2\beta + (\frac{1}{2}\beta)^2$. At high densities $\rho\lambda_0^3 > 30$, a (roughly circular) hole appears in the distribution $p(\lambda)$ on the complex plane. The density at which the hole appears does not depend on β . The marginal probability distribution of $\text{Re}\lambda$ is described by our equation (32) at all β , provided that $\rho\lambda_0^3 < 30$. The marginal distribution of $\text{Im}\lambda$ follows the Marchenko-Pastur law (21) for $\frac{1}{2}\beta < 1$ and decays as $1/|\text{Im}\lambda|$ at larger β .

Finally, we studied a model matrix $\hat{X} = \hat{C} + i(\hat{S}' - \hat{\mathbb{I}})$ in which two independent ensembles of points $\{\mathbf{r}_i\}$ and $\{\mathbf{r}'_i\}$ were used to generate matrices \hat{C} and \hat{S}' . The matrices \hat{C} and \hat{S}' are asymptotically free and the distribution of eigenvalues of \hat{X} at $\beta < 1$ can be found using the approach developed by Jarosz and Nowak [29] based on the theory of free random variables. The distribution of eigenvalues shows an interesting transition from a circular shape at $\beta \ll 1$ to a triangular shape at $\beta \sim 1$, and then to an ‘inverted T’ shape for $\beta \gg 1$.

References

- [1] Mehta M L 1991 *Random Matrices* (New York: Academic)
- [2] Beenakker C W J 1997 *Rev. Mod. Phys.* **69** 731
- [3] Fyodorov Y V and Sommers H J 1997 *J. Math. Phys.* **38** 1918
- [4] Guhr T, Müller-Groeling A, Weidenmüller H A 1998 *Phys. Rep.* **299** 189
- [5] Mézard M, Parisi G and Zee A 1999 *Nucl. Phys. B* **559** 689
- [6] Parisi G 2006 in *Applications of Random Matrices in Physics. NATO Science Series, Series II: Mathematics, Physics and Chemistry* **221** 219
- [7] Rusek M, Orłowski A and Mostowski J 1996 *Phys. Rev. E* **53** 4122
- [8] Rusek M, Mostowski J and Orłowski A 2000 *Phys. Rev. A* **61** 022704
- [9] Pinheiro F A, Rusek M, Orłowski A and Van Tiggelen B A 2004 *Phys. Rev. E* **69** 026605
- [10] Antezza M, Castin Y and Hutchinson D arXiv:1006.4429
- [11] Ernst V 1969 *Z. Phys.* **218** 111

- [12] Svidzinsky A and Chang J T 2008 *Phys. Rev. A* **77** 043833
- [13] Scully M O 2009 *Phys. Rev. Lett.* **102** 143601
- [14] Svidzinsky A A and Scully M O 2009 *Opt. Commun.* **282** 2894
- [15] Svidzinsky A A, Chang J T and Scully M O 2010 *Phys. Rev. A* **81** 053821
- [16] Akkermans E, Gero A and Kaiser R 2008 *Phys. Rev. Lett.* **101** 103602
- [17] Pinheiro F A and Sampaio L C 2006 *Phys. Rev. A* **73** 013826
- [18] Goetschy A and Skipetrov S E (in preparation)
- [19] Labeyrie G, De Tomasi F, Bernard J C, Müller C A, Miniatura C and Kaiser R 1999 *Phys. Rev. Lett.* **83** 5266
- [20] Labeyrie G, Vaujour E, Müller C A, Delande D, Miniatura C, Wilkowski D and Kaiser R 2003 *Phys. Rev. Lett.* **91** 223904
- [21] Lagendijk A, Van Tiggelen B, Wiersma D S 2009 *Physics Today* **62**(8) 24
- [22] Voiculescu D V, Dykema K J and Nica A 1992 *Free Random Variables* (Providence, RI: American Mathematical Society)
- [23] Tulino A M and Verdú S 2004 *Random Matrix Theory and Wireless Communications* (Delft: Now Publishers)
- [24] Marčenko V A and Pastur L A 1967 *Mat. Sbornik (USSR)* **1** 457
- [25] Zee A 1996 *Nucl. Phys. B* **474** 726.
- [26] Janik R A, Nowak M A, Papp G, Wambach J and Zahed I 1997 *Phys. Rev. E* **55** 4100
- [27] Feinberg J, Zee A 1997 *Nucl. Phys. B* **504** 579
- [28] Feinberg J 2006 *J. Phys. A: Math. Gen.* **39** 10029
- [29] Jarosz A and Nowak M A 2006 *J. Phys. A: Math. Gen.* **39** 10107
- [30] Chalker J T and Mehlig B 1998 *Phys. Rev. Lett.* **81** 3367
- [31] <http://www.netlib.org/lapack/>
- [32] Haake F, Izrailev F, Lehmann N, Saher D, Sommers H J 1992 *Z. Phys. B* **88** 359
- [33] Lehmann N, Saher D, Sokolov V V, Sommers H J 1995 *Nucl. Phys. A* **582** 223